PCCP

Accepted Manuscript

This article can be cited before page numbers have been issued, to do this please use: P. Y. Steinberg, M. M. Zalduendo, G. Giménez, G. J. D. A. A. Soler-Illia and P. C. Angelomé, *Phys. Chem. Chem. Phys.*, 2019, DOI: 10.1039/C9CP01896D.

ROYAL SOCIETY OF CHEMISTRY

rsc.li/pccp

View Article Online
DOI: 10.1039/C9CP01896D

TiO_2 mesoporous thin films architecture as a tool to control Au nanoparticles growth and sensing capabilities

Paula Y. Steinberg[1,§], M. Mercedes Zalduendo[1,§], Gustavo Giménez[2], Galo J. A. A. Soler-Illia[3], Paula C. Angelomé[1,*]

[1] Gerencia Química, Centro Atómico Constituyentes, Comisión Nacional de Energía Atómica, CONICET, Av. Gral. Paz 1499, B1650KNA San Martín, Buenos Aires, Argentina.

[2] Centro de Micro y Nanoelectrónica del Bicentenario, INTI-CMNB, Instituto Nacional de Tecnología Industrial, San Martín, Buenos Aires, Argentina

[3] Instituto de Nanosistemas, UNSAM, CONICET, 25 de mayo 1021, 1650 San Martín, Buenos Aires, Argentina.

[§] These authors contributed equally to this work

[*] Corresponding author, email: angelome@cnea.gov.ar

ABSTRACT

In this paper, a systematic study about the effect of mesoporous structure over Au nanoparticles (NPs) growth inside and through the pores of TiO_2 mesoporous thin films (MTTFs) is presented and the effect of such characteristics over the composites' sensing capabilities is evaluated. Highly stable MTTFs with different pore diameters (4 – 8 nm range) and pore arrangements (body centered and face centered cubic) were synthesized and characterized. Au NPs were grown inside the pores, and it was demonstrated, through a careful physicochemical characterization, that the amount of incorporated Au and the NPs size depends on the pore array, being higher for bigger pore's diameters and face centered cubic structures. The same structure allows the growth of more and longer tips over Au NPs deposited in the thin film/substrate interface. Finally, to confirm the effect of the composites structural characteristics over their possible applications, the materials were tested as Surface Enhanced Raman Scattering (SERS) spectroscopy substrates. The composites with the higher amount of Au and more ramified NPs were the ones that presented the better sensitivity in the detection of a probe molecule (*p*-nitrotiophenol). Overall, this work demonstrates that the pore size and ordering in MTTF determines the materials' accessibility and connectivity and thus has a clear effect over their potential applications.

View Article Online
DOI: 10.1039/C9CP01896D

INTRODUCTION

Nowadays the use of mesoporous thin films (MTF) and their composites with metallic nanoparticles as active or constitutive part of advanced devices is being extensively studied by the scientific community.[1-4] The choice of these kind of materials is based on the individual properties of each component and the new ones that appear due to their combination.

In particular, MTF feature a highly ordered array of monodisperse mesopores whose diameter can be controlled in the 2 - 10 nm range. The mesoporosity gives rise to a high specific surface area in contact with the medium and thus, it is available for physicochemical interactions.[3, 5, 6] Metallic nanoparticles (NPs), on the other hand, are one of the most studied families of nanomaterials, due to their optical and catalytic properties.[7, 8] These properties are derived from their high surface to volume ratio, the existence of the so called localized surface plasmon resonances (LSPR) and the high electric field enhancements at the NPs´ surface.[9, 10]

Today, thanks to the advance of nanomaterials' chemistry, it is possible to carefully control a wide variety of characteristics of MTF, metallic NPs and the composites that contain both materials. The chemical composition can be selected from the synthesis, allowing the obtention of pure and mixed oxides or hybrid organic-inorganic materials in the case of MTF, and a wide variety of metals and alloys in the case of NPs. Moreover, the size and shape of the NPs can be tuned[11, 12] and also the pore size and distribution can be designed for the MTF.[3, 6] In the same way, the location of each component in the material can be controlled when composites are designed.[1, 2, 4]

As indicated before, many applications for MTF and their composites with metallic NPs are under development nowadays. Such applications include sensing devices, catalysts, photocatalysts, and several optical devices.[1, 2, 4, 13] In particular, our group has extensively demonstrated the feasibility of using NPs-MTF composites as substrates for trace-molecules detection by Surface Enhanced Raman Scattering (SERS) based spectroscopy.[14] Au and Ag NPs were tested, included within or covered by TiO_2 and SiO_2 mesoporous thin films.[15-18] However, for each of the tested systems, only one kind of mesoporous architecture was studied and no careful comparison between different pore sizes or pore ordering were made. Nevertheless, it is clear that the porous structure of the MTF should affect the final properties of the any device built using them as a key component.

Several studies are found in the literature about the effect of the mesoporous structure over accessibility and reactivity of MTF. For example, Walcarius' group has demonstrated, through cyclic voltammetry measurements, that the organization of SiO_2 MTF porous network has a profound

View Article Online
DOI: 10.1039/C9CP01896D

effect on its permeability properties.[19] For the same material, Hillhouse's group measured MTF accessibility and species diffusivity through the pores, and found that the degree of order and pore orientation in the film, in addition to its symmetry, are dominant factors that determine those key parameters.[20] Electrochemical measurements were also used to demonstrate that morphological transformations generated by thermal treatment of TiO_2 MTF have clear consequences over the accessibility of the material.[21] Similar techniques were used to probe that permeability of TiO_2 MTF can be tuned by adding bimodal porosity.[22] Moreover, it has been demonstrated through microscopy measurements that the solvent's filling of TiO_2 MTF depends on the pore ordering.[23] And, for similar systems, it has been demonstrated by Fluorescence Correlation Spectroscopy measurements that pores and necks sizes affect a dye diffusion coefficient inside the MTF.[24] Interestingly, besides the permeability and accessibility studies, it was shown that the pore architecture affects the photocatalytic activity of crystallized TiO_2 MTF[25] and the load and release of cargo molecules from the pores of SiO_2 MTF.[26]

In the case of composites materials, our group has demonstrated that the pore architecture of silica MTFs affects the way Au NPs growth through them.[27] In the same sense, it has also been demonstrated that metallic NPs growth inside MTF can be affected by the pore architecture.[28, 29] For example, it has been shown that Ag can grow as nanospheres or nanorods, depending on the pore ordering of SiO_2 mesostructured films (*i.e.* with pores filled with organic template).[30] Such differences over the metallic NPs growth have consequences over the final properties of the composite. In particular, it has been shown that electrochemical sensing activity,[31, 32] electrical conductivity,[33] and nonlinear optical properties[34] depend on the mesoporous size, interconnectivity and accessibility.

Although all the presented examples points towards an effect of the mesoporosity over accessibility and connectivity, most of them have been performed on SiO_2 MTFs and no systematic studies relating pore architecture of TiO_2 MTFs are found in the literature. Moreover, no specific relation between pore architecture and sensing capabilities has been presented so far for these systems.

In this paper, a systematic study over the effect of mesoporous structure on Au NPs growth both inside and through the pores of TiO_2 MTF with different pore sizes and pore ordering is presented. To the best of our knowledge, this is the first time three TiO_2 systems MTF are presented together as different nanosized environments to study the effect of their structures over Au NPs growth. As mentioned before, the accessibility and connectivity of TiO_2 MTF has not been studied in deep, but this oxide presents several advantages from the applications point of view, including high chemical

View Article Online
DOI: 10.1039/C9CP01896D

stability and the availability of several procedures to obtain it with different porous architectures. In the same sense, Au NPs were selected due to their optical properties and the chemical inertness of the metal. In a first step, the effect of the porous structure and pore size over the growth of Au NPs was evaluated through a careful physicochemical characterization, and compared with the previously obtained results for one of the presented architectures.[18] These measurements allowed to relate the structural characteristics of the MTF with the structure and/or arrangement of the Au NPs grown inside or through the pores. Afterwards, to confirm the effect of the composites structural characteristics over their possible applications, the obtained composites were tested as SERS substrates.

EXPERIMENTAL SECTION

Materials. Titanium tetrachloride ($TiCl_4$) and Brij 58 ($CH_3(CH_2)_{15}(CH_2CH_2O)_{20}OH$) were supplied by Merck. Titanium tetraethoxide (TEOT), Pluronic F127 ($HO(CH_2CH_2O)_{106}(CH_2CH(CH_3)$-$O)_{70}(CH_2CH_2O)_{106}OH$) and Pluronic P123 ($HO(CH_2CH_2O)_{20}(CH_2CH(CH_3)$-$O)_{70}(CH_2CH_2O)_{20}OH$), tetrachloroauric(III) acid trihydrate ($HAuCl_4 \cdot 3H_2O$), (3-aminopropyl)trimethoxysilane (APTES), cetyltrimethylammonium bromide (CTAB), trisodium citrate dihydrate, sodium borohydride ($NaBH_4$) and ascorbic acid (AA) were purchased from Sigma-Aldrich. Hydrogen peroxide (H_2O_2, 28%) was supplied by Biopack, sulfuric acid (H_2SO_4, 98%) by Cicarelli, and para-nitrothiophenol (pNTP, 80%) by Acros-Organics. Phosphate buffer saline (PBS) 0.5 M pH 7.4 was obtained by mixing Na_2HPO_4 (Biopack) and NaH_2PO_4 (Merck). NaOH and HCl (both purchased from Merck) solutions were added to adjust pH when required. All chemicals were used as received. Absolute ethanol (Biopack) and Milli-Q water (R = 18 $M\Omega.cm^{-1}$) were used as solvents or reactants.

Gold nanoparticles synthesis and immobilization. Citrate-stabilized gold nanospheres of 66 nm diameter were prepared according to a previously reported procedure.[35] Immobilization of the synthesized Au NPs was carried out by immersion of APTES-functionalized glass slides into the gold NPs suspensions (as obtained, without purification) for 40 minutes. APTES-functionalized glass slides were prepared by a two-step procedure. First, glass slides were activated using freshly prepared piranha solution (3:1 mixture of H_2SO_4 and 30% H_2O_2) for 1 hour. Secondly, the surface was functionalized by dipping the dry glass slides in a 0.01 M APTES solution in pure grade ethanol, for 3 h.

View Article Online
DOI: 10.1039/C9CP01896D

Mesoporous titania thin film synthesis. Titania MTF were produced by the well-known Evaporation Induced Self Assembly approach, that combines sol-gel reactions (that give rise to the oxide) and surfactants self-assembly, that give rise to the pores.[36] Precursor sols were prepared as reported elsewhere[37, 38] by mixing $TiCl_4$ or TEOT, absolute ethanol, pore template (Brij 58, Pluronic F127 or Pluronic P123), HCl and Milli-Q water. The molar compositions of the sols are indicated in Table 1. Titania systems were labeled TB, TF and TP depending on the surfactant used as pore template: Brij 58, F127 and P123, respectively. Samples in which pre-deposited Au NP were covered by TiO_2 films were labeled *Au66/T**X***, where **X** refers to the different templates.

Table 1: Molar composition of the sols prepared in this work

System	$TiCl_4$	TEOT	Template	Ethanol	HCl	H_2O	Withdrawal speed (mm/s)	Spinning speed (rpm)
TB	1	0	0.050	40.0	-	10.0	1.5	2000
TF	1	0	0.005	40.0	-	10.0	1	8000
TP	0	1	0.014	44.7	1.99	6.9	2	4000

Thin films were produced by either dip-coating onto cleaned glass slides or by spin-coating onto Au NP-modified glass slides. The withdrawal speed and spinning speed were adjusted in the ranges 1-2 mm s^{-1} and 2000-8000 rpm, respectively, to obtain films with similar thickness. After deposition, films were stabilized using a four steps procedure: 24 h at room temperature in a 50% relative humidity chamber, 24 h at 60 °C, 24 h at 130 °C and 2h at 200 °C (temperature rate from 130 to 200 °C was 1 °C min^{-1}). Finally, films were immersed in ethanol for 3 days to remove the pore template.

Nanoparticle Seeded Growth. Anisotropic growth of the Au NPs below the different mesoporous films was achieved following a reported method.[18, 27] Briefly, the above mentioned *Au66/TX* samples were immersed for two hours in a $HAuCl_4$:CTAB:AA solution with a molar ratio of 1:60:16 and a [Au (III)] = 6.25×10^{-5} M. This two hours growth step was repeated 3 times. After each step, samples were rinsed with water and air-dried. The obtained composites were labeled *Au66**NS**/TX*, since the NPs shape resembles nanostars (NS) shape.

Gold nanoparticles synthesis inside TiO_2. Synthesis of Au NPs inside mesoporous titania thin film was carried out according to a previously reported method.[18, 39] The synthesis occurs through an adsorption-reduction procedure called reduction step (RS). In the first place, the film was immersed for 1 minute in a 1 mM solution of $HAuCl_4 \cdot 3H_2O$ at pH 4 to allow the adsorption of $AuCl_3(OH)^-$ on

View Article Online
DOI: 10.1039/C9CP01896D

the positively charged surface of TiO_2.[40] After this time, the film was rinsed with water and air-dried. Afterwards, the film was dipped for 1 minute in a 5 mM $NaBH_4$ freshly prepared solution, for the reduction of adsorbed Au(III). Finally, the film was rinsed with water. The complete process was repeated as many times as desired in order to increase the filling fraction of the mesoporous framework. The samples were labeled *Au**Z**RS@TX*, where **Z** refers to the number of RSs that the film was submitted to. For example, Au5RS@TB refers to a TB film subjected to 5 RSs.

Characterization.

Optical characterization. A HP Agilent 8453 spectrophotometer was used to record UV−vis−NIR spectra.

Grazing incidence Small Angle X-Ray Scattering (GISAXS) measurements. GISAXS patterns were obtained at the SAXS beamline in Elettra synchrotrone (Trieste, Italy). X-ray with a 1.54 Å (8 keV) wavelength were used. Samples were placed at 86.244 cm from a Pilatus 1M detector. This distance was calibrated with a silver behenate standard.

Electron Microscopy. Transmission electron microscopy (TEM) analysis was carried out by using a Philips CM 200 microscope operating at 180 kV. Samples were scratched from the substrate and deposited on FORMVAR/carbon-coated copper grids. Scanning electron microscopy (SEM) was performed using a Carl-Zeiss SUPRA 40 microscope. Films were cut into smaller pieces and positioned parallel to the holder to analyze its surface, and perpendicular to the holder to observe NPs underneath the film and/or NPs along the film thickness. Energy-dispersive spectroscopy (EDS) was executed in a Philips SEM microscope equipped with an EDAX detector. For this analysis, samples were scratched off from the substrate and placed on adhesive carbon tape.

Further sample preparation for cross section analysis was performed using a Helios NanoLab 650FEI Focused Ion Beam-Scanning Electron Microscopy (FIB-SEM). For this preparation the Au NPs and film were deposited onto a silicon substrate instead of glass. Localized Pt thin film (150 nm)) was deposited on the sample to protect it, and gallium ion column were used to prepare a lamella of the portion of interest. The obtained piece, with a final thickness of about 30 nm was welded to a FIB-TEM copper grid and analyzed by means of that technique.

X-ray reflectometry (XRR). XRR studies allow the determination of films´ porosity and thickness, as well as Au loading fraction.[18, 28] A Panalytical Empyrean X-Ray diffractometer with an incident beam of Cu K_α radiation at 1.54 Å was used for XRR measurements. Measurements were performed with an incident angle of 1°, a mask of 10 mm and a divergence slit of 0.38 mm. More details about

View Article Online
DOI: 10.1039/C9CP01896D

thickness determination, porosity and Au filling fractions calculations are presented in the Supporting Information.

SERS experiments and analysis. Samples of about 0.5 x 0.5 cm^2 were immersed in 1mL of pNTP $4x10^{-4}$ M (solvent: PBS pH 7.4). The incubation was carried out overnight in the fridge, then samples were rinsed with water and air-dried. A Horiba LabRAM HR Raman system (Horiba JobinYvon) with a confocal microscope in backscattering geometry was used for measurements. A 632.8 nm laser was chosen as the excitation source with a power output of 12 mW, therefore appropriate filter optics were used to avoid probe degradation. All measurements were performed in confocality mode with a 100 µm pinhole and a 100x objective with a numerical aperture value of 0.9. A 600 grooves mm^{-1} grating was used. Acquisition times were varied between 5 s and 60 s (1 scan). Spectra were taken from at least 10 different points in each sample. For comparative studies, the parameters chosen were spectra intensities and minimum acquisition time. The latter, defined as the minimum time required to see S > 3 N (signal three times greater than noise) in at least 90% of the tested points, is use as a relative parameter to determine platform´s sensitivity.[18]

RESULTS AND DISCUSSION

Mesoporous TiO_2 thin films characterization – *TX* systems. Mesoporous TiO_2 thin films (MTTFs) were obtained as previously reported.[37, 38] All the obtained samples presented a good optical quality: transparent, homogeneous and crack-free. After thermal treatment and removal of the pores' templates, all MTTFs presented similar thickness (150-180 nm, see Table S1). GISAXS patterns (Figure 1 D, E and F), together with SEM images (Figure 1 G, H and I), demonstrate that TB and TF systems present a body centered cubic *Im3m* porous structure with the (110) planes parallel to the substrate, as depicted in Figure 1A and B. TP films, on the other hand, show a pore structure compatible with a face centered cubic $Fm3m$ symmetry with the (111) planes parallel to the substrate, as depicted in Figure 1C. These results are in accordance with previously reported ones.[37, 41-43] From SEM images (Figure 1 G, H and I) it was determined that the TB films presented the smallest pore diameter (4 ± 1 nm), below the pore size of TF system (8 ± 1 nm). TP films, on the other hand, presented a pore diameter of 9 ± 1 nm, comparable to the pore diameter of TF films. It is important to highlight that, as a consequence of thermal treatment, the MTTFs shrink in the direction perpendicular to the substrate, improving the connection between consecutives pores through necks.[6, 42] For this films, treated at 200 ºC, the necks presented a diameter of 1.8 ± 0.2 nm

View Article Online
DOI: 10.1039/C9CP01896D

for TB, 2.1 ± 0.2 nm for TF and 3.4 ± 0.8 nm for TP samples, as determined by Environmental Ellipsometric Porosimetry (see SI for details).

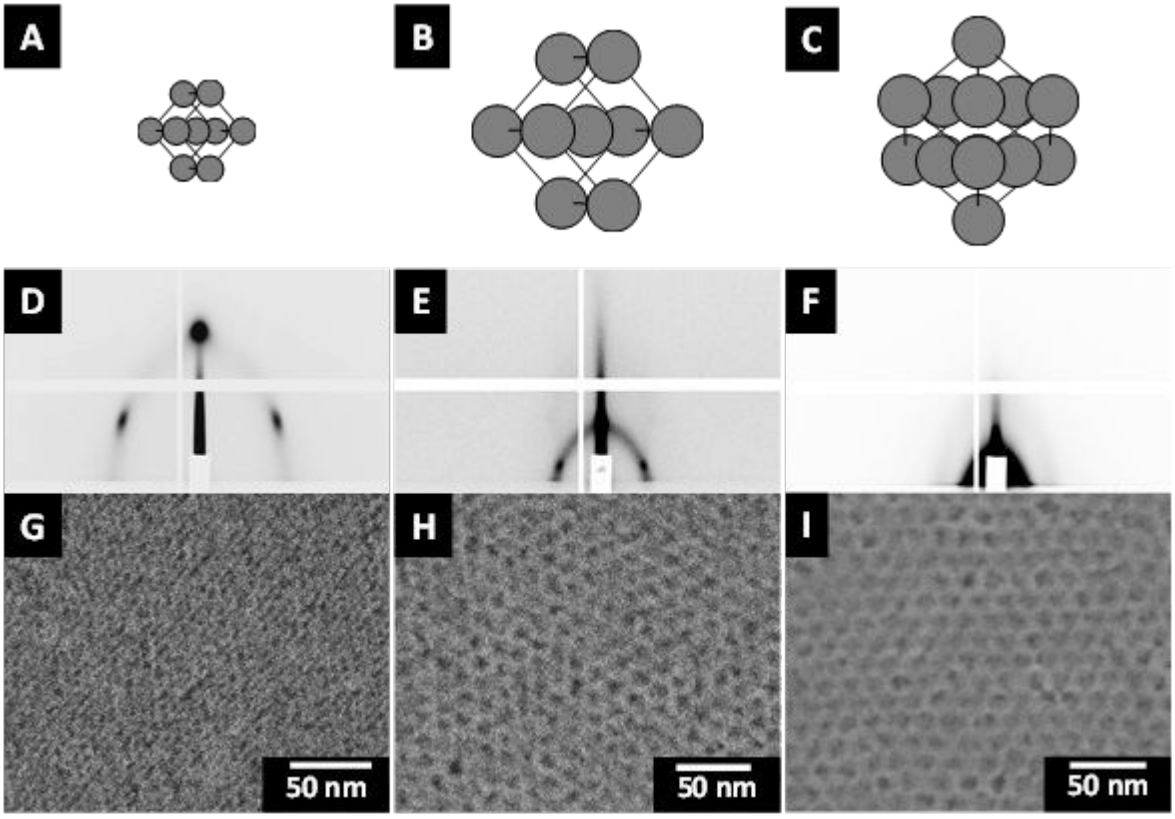

Figure 1. Schematic representation of tridimentional porous structures obtained in this work: cubic *Im3m* with two pore sizes **(A and B)** of TB and TF films, respectively and cubic *Fm3m* **(C)** of TP films. GISAXS patters for **(D)** TB, **(E)** TF and **(F)** TP mesoporous films. SEM images of film surface for **(G)** TB, **(H)** TF and **(I)** TP systems.

Thus, two simple comparison can be made with the chosen systems: TB *vs* TF, where the pores diameter change without changing the porous structure and TF *vs* TP, where the pores diameter is similar but the pores ordering is different. Finally, it worth noting that when necks diameters are taken into account, TP system is unique since it has the highest value for this parameter. All these comparison will be taken into account in the following sections.

Synthesis of Au NPs inside mesoporous TiO_2 thin films – *AuZRS@TX* systems

Gold NPs synthesis inside mesoporous TiO_2 thin films was performed as previously reported, using an adsorption-reduction approach.[18, 39] In this approach, Au (III) is adsorbed over the TiO_2 walls and

View Article Online
DOI: 10.1039/C9CP01896D

is subsequently reduced by means of $NaBH_4$. Thus, the particles growth inside the pores, as schematized in Figure 2A. This adsorption-reduction procedure can be repeated several times, to increment the Au loading inside the films. When Au NPs were grown by this means over the three different TX films, each sample presented a different color, as depicted in Figure 2B. This color is related with a distinctive plasmonic band maximum and width (Table S2), as can be seen in the UV-visible absorption spectra of the samples, presented in Figure 2.

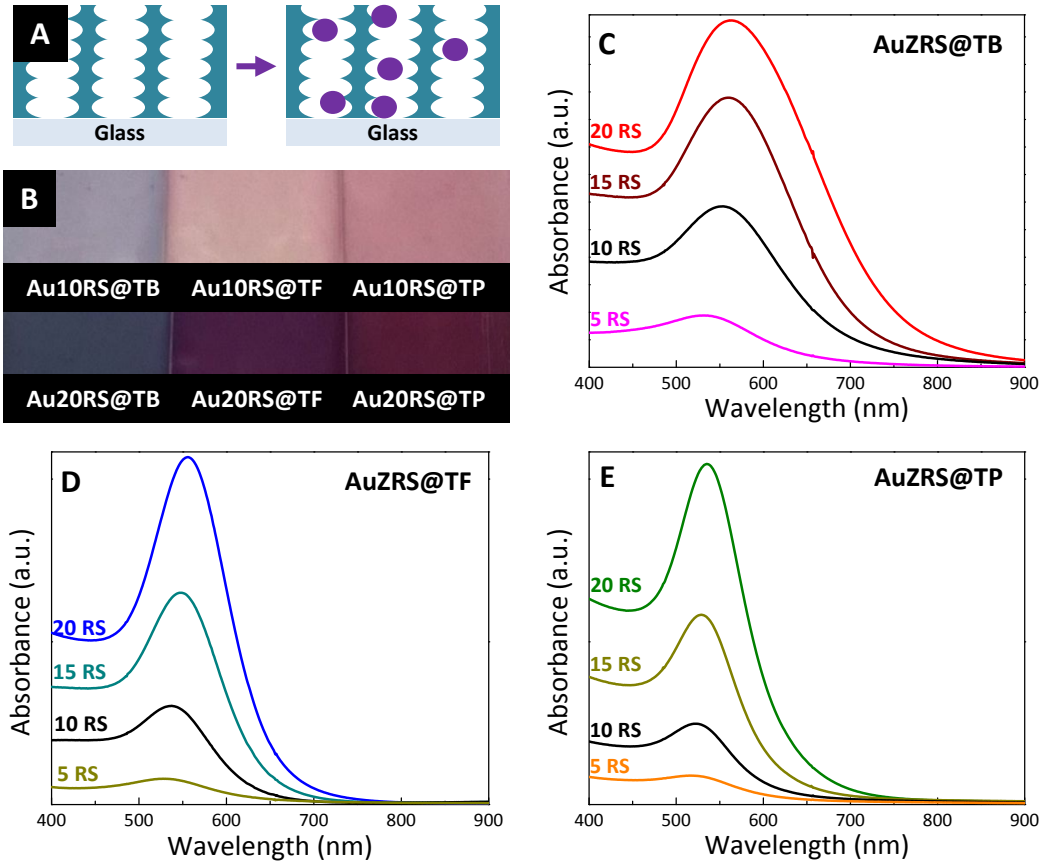

Figure 2. (A) Schematic representation of MTTF before and after Au NPs synthesis inside the pores. **(B)** Optical image of *AuZRS@TiO₂* samples (*Z* = 10 and 20). UV-visible spectra of *AuZRS@TiO₂* samples (*Z* = 5, 10, 15 and 20) for **(C)** TB, **(D)** TF and **(E)** TP.

As a general behavior, a well-defined plasmonic band gradually develops as the Au NPs synthesis proceeds (*i.e.* when the number of RS is increased). This plasmonic band corresponds to Au NPs surrounded by a high refractive index dielectric medium. In all cases, a change in the plasmonic band

View Article Online
DOI: 10.1039/C9CP01896D

intensity and a maximum's red-shift is observed when the number of RS is incremented from 5 to 20. This behavior can be attributed to an increase in number and size of the NPs, as formerly observed for TF system.[18] However, significant differences are identified in the UV-visible spectra of the three mesoporous architectures loaded with Au NPs.

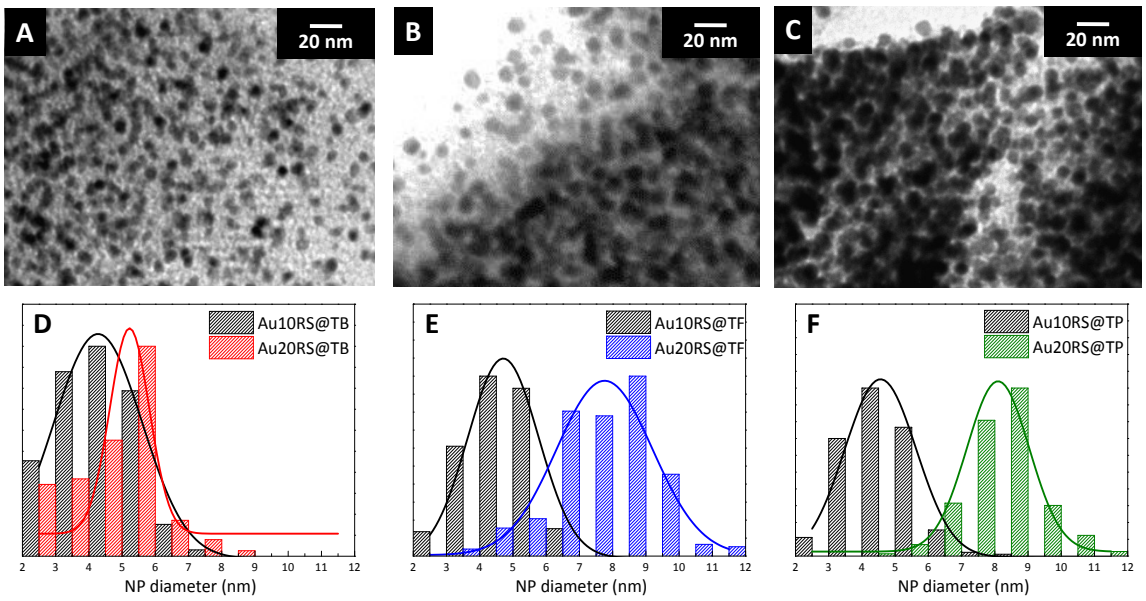

Figure 3. TEM images of **(A)** Au20RS@TB, **(B)** Au20RS@TF, and **(C)** Au20RS@TP samples. NPs size histograms for **(D)** *AuZRS@TB*, **(E)** *AuZRS@TF*, and **(F)** *AuZRS@TP* samples (*Z*= 10 and 20).

From TEM micrographs (Figure 3 A, B and C and Figure S1), it can be seen that NPs, visualized as dark spots, are spheroidal and evenly distributed in the films. SEM micrographs (Figure S2) also show that NPs are uniformly dispersed through the films thickness. Size analysis from TEM images (Figure 3 D, E and F) reveals that in all cases NPs grow when the number of RS is increased from 10 to 20. In fact, when 10 RS are carried out, NPs mean diameter is similar for the three architectures: 4 ± 1 nm (for Au10RS@TB) and 5 ± 1 nm (for Au10RS@TF and Au10RS@TP). However, when 20 RS are carried out, dissimilarities arise. NPs size is smaller in the system with the lower pore size: TB (5 ± 1 nm) than in the case of the films with bigger pore sizes: TF and TP (8 ± 1 nm). Hence, it can be concluded that the Au NPs' growth is restricted by the matrix, as was previously observed for Ag NPs growth.[28] Interestingly, when the histograms for Au20RS@TF and Au20RS@TP samples are compared, a higher particles size dispersion is observed for TF based samples. This behavior is probably related to the fact that NPs growth also inside the necks between the pores. For TP

View Article Online
DOI: 10.1039/C9CP01896D

samples, the pores and the necks are closer in diameters and for TF the sizes are more dissimilar. Thus the final size dispersion of NPs grown inside TP films results smaller.

As shown above, NPs are spheroidal and their diameters are in the 4-8 nm range for all samples. Therefore, the position of the plasmonic band maximum is primarily a consequence of the environment that surrounds the NPs, and the plasmonic band width is mainly a result of NPs proximity. To start with, the average refractive index in each case results from the combination of the TiO_2 walls and air, given by the film´s porosity (see Table S1 for values). TP films present the lowest average refractive index (*i.e.* the higher porosity, if the refractive index of TiO_2 walls is considered equivalent in all systems). Consequently, Au NPs included within TP (*AuZRS@TP* samples) have the lowest plasmonic band maximum position. On the other hand, TF films present a slightly lower average refractive index than TB, therefore the plasmon band in *AuZRS@TF* samples is blue-shifted with respect to the one of *AuZRS@TB* samples. Moreover, *AuZRS@TB* samples feature a broader plasmonic band compared to *AuZRS@TF* and *AuZRS@TP* samples. A plausible explanation is the proximity of Au NPs located in the TB matrix as a result of the shorter interpore distance in this kind of film. Thus, not only the pore size but also the pore distance plays a key role over the NPs interaction within the oxide's structure.

Finally, to complete the understanding of the Au filling process inside the different architectures, XRR (Figure S3 and Table S3) and EDS measurements (Table S4) were carried out. These results show that, for the same quantity of RS, the fraction of Au within the material is greater in the most porous and interconnected system TP (11% for 20 RS) than in TF (9%). When the same architecture (*Im3m* cubic) is compared but the pore sizes is changed, it can be seen that lower filling is observed for the system with smaller pores TB (7% of the porosity is occupied). Therefore, these results demonstrate that the amount of gold that can be incorporated inside the films is controlled by the mesostructure and its accessibility.

The synthesis of Au NPs inside these three architectures shows that all the systems are accessible to reactants and allow reactions to take place. The reactivity is different for each mesostructure and depends on pore arrangement and dimensions. In particular, TB system presents the smallest NPs diameter, limited by the film´s pore and neck diameters and the lowest incorporation of gold, restricted by the low accessibility. TP system, on the other hand, presents the largest pores and necks and incorporates a larger amount of gold, allowing a greater NPs growth. Finally, TF system can accommodate NPs with similar size than TP system, but a lower amount of gold incorporated.

View Article Online
DOI: 10.1039/C9CP01896D

Such lower accessibility is attributed to the fact that the pores in the TF body centered cubic structure are less interconnected between them than in the case of TP's face centered cubic one (see Figure 1 B and C for this comparison). Moreover, it is important to highlight that once NPs have grown, all systems, independently on their architecture, are still accessible to water vapor (see Figure S4) and thus, to analytes.

Overgrowth of Au NPs placed below mesoporous TiO_2 thin films – *Au66NS/TX* systems

As has been previously demonstrated, another interesting possibility regarding the combination of Au NPs and MTTF is to place the particles in between the substrate and the film and to grow them through the porosity afterwards, as schematized in Figure 4A. In this case, it is important to first confirm that the MTTF properties deposited on top of the Au NPs modified substrate are equivalent to the ones of the films deposited on bare substrates. GISAXS measurements were used for such purpose (Figure S5), demonstrating that for the three tested architectures the pore arrangement is not affected due to the presence of the NPs. These results are in agreement with those previously obtained for silica films and multilayered systems.[27, 44] Regarding the film thicknesses, they are still in the same range (180-200 nm, Table S5 and Figure S6), although some differences are observed due to the fact that spin coating was used to prepare Au66/TX samples, instead of dip coating procedure used for TX samples. Moreover, the films are smooth over the Au NPs (Figure S6). Concerning the optical properties, a clear color difference between *Au66/TX* samples was observed (Figure 4C). *Au66/TB* samples presented a blue color while *Au66/TF* and *Au66/TP* had a pink-red color. This color change corresponds with the UV-visible spectrum of each sample (Figure 4B). Plasmonic band maximum position trend (*Au66/TP* < *Au66/TF* < *Au66/TB*, see Table S6) is in agreement with the averaged refractive index of the different TiO_2 mesoporous films (TP < TF < TB) that surround the NPs (see values in Table S5). Thus, the pink color is more intense when the film on top is more porous (*i.e.* presents a lower refractive index) and a more intense violet color develops when the film on top is less porous.

After characterizing the systems, the selective growth of Au NPs placed below MTTFs was achieved following a previously reported method that involves the selective reduction of Au (III) by means of ascorbic acid, over the original Au NPs.[15, 18] In this point, it is important to highlight that the

View Article Online
DOI: 10.1039/C9CP01896D

overgrowth of Au NPs covered with mesoporous thin films has already been reported for mesoporous SiO_2[27] and TF[15, 18] but not for TB and TP systems.

Figure 4B shows the UV-visible spectra of samples after the Au NPs overgrowth. When Au NPs covered with MTTFs are overgrown, a second plasmonic band appears at higher wavelengths, and thus, a difference in color can be appreciated (Figure 4C). This is indicative of a change in NPs morphology, hinting that the three architectures allow the diffusion of molecules from solution to the bottom of the film where the NPs are placed. In fact, the spectra of *Au66NS/TX* samples resemble the ones of nanostars or nanoflowers, in which two partially superimposed plasmonic bands can be described: the one attributed to the core (at lower wavelengths) and the one attributed to the tips (at higher wavelengths).[45]

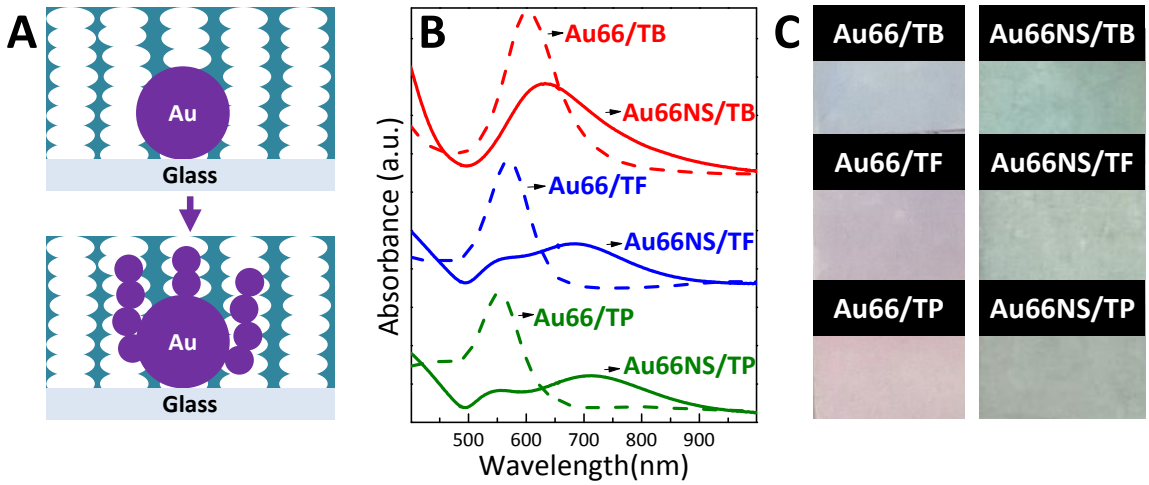

Figure 4. (A) Schematic representation of Au NPs covered with MTTF before and after Au NPs overgrowth. **(B)** UV-visible spectra of *Au66/TX* (dashed line) and *Au66NS/TX* samples (solid line); **(C)** Optical image of *Au66/TX* and *Au66NS/TX* samples.

NPs final morphology can be seen in TEM images in Figure 5; Figure S6 present TEM images before NPs overgrowth for comparison.

View Article Online
DOI: 10.1039/C9CP01896D

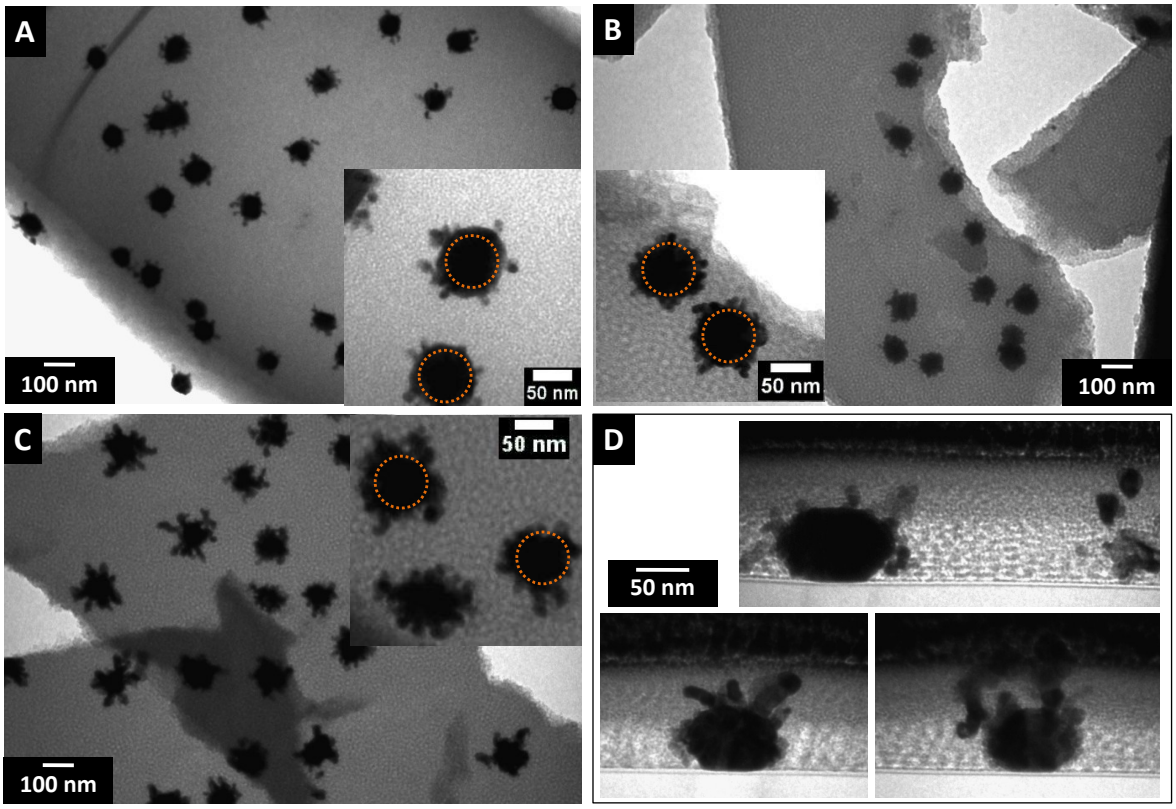

Figure 5. TEM images of **(A)** Au66NS/TB, **(B)** Au66NS/TF, and **(C)** Au66NS/TP. The inset images present a higher magnification and the dashed circles are a guide to the eye to represent the original 66 nm Au NP used as seed. **(D)** TEM images of the Au66NS/TF sample cross-section lamella prepared by FIB.

As a first observation, it is evident that all NPs covered with the different films have grown. Furthermore, NPs growth is anisotropic since it can only occur through the pores that surround them: Figure 5D clearly shows that tips grow through the porosity and not in the direction of the substrate. Moreover, TEM images show that anisotropic growth is different for each tested architecture. This growth can be qualitatively estimated by measuring an effective tip length from the TEM images, since they show a two-dimensional projection of the tridimensional growth. By doing that, it can be seen that NPs grown through TP films display the longest effective tips (60 ± 27 nm) in a highly branched structure, whereas NPs grown in TB films present the shortest effective tips (13 ± 7 nm). NPs grown in TF film, on the other hand, present an intermediate effective tips size (21 ± 11 nm) between the three systems (see Figure S7 for histograms of effective tips sizes distribution). This differential NPs overgrowth can be interpreted taking into account the

View Article Online
DOI: 10.1039/C9CP01896D

combination of precursors accessibility and the possibility of the tips to grow through the structure, both given by the pore´s dimensions and interconnection. It is clearly seen that NPs growth is controlled by the film´s characteristics: TP films allow a greater ramified growth due to the combination of bigger and more interconnected pores while NPs growth is restricted in TB films with smaller and less interconnected pores. For TF films an intermediate behavior is observed, due to the fact that the pore size is close to the TP films but the pore ordering is the same as in TB films. Interestingly, previous results of NPs overgrowth below SiO_2 mesoporous thin films templated with Brij 58 (equivalent to TB samples) resulted in almost spherical Au NPs, probably due to the local dissolution of the SiO_2 walls that surrounds them.[27] Consequently, the results obtained in this work demonstrate that titania´s higher chemical stability[46] presents a benefit when anisotropic growth is envisioned.

Sensing capabilities of the obtained structures

Since the different MTTFs gave rise to very distinctive Au NPs architecture and their size, shape and proximity vary in all of them, an effect over the composites properties is expected. These different properties will sure have consequences over the composites' possible applications. To test such hypothesis, the use of the composites as SERS substrates was selected. SERS is a very powerful technique that allows trace-molecule detection, by taking advantage of the amplification of the Raman signals in the presence of metallic nanostructures.[14] The use of NPs-MTF composite as SERS based sensors was previously demonstrated[15-17, 47, 48] and our group has recently presented a careful characterization of AuNPs-TF systems, that serves as a base for the experiments presented here.[18] Hence, SERS sensing capabilities of all synthesized composites were studied in a comparative way, using pNTP as probe molecule. SERS spectra were taken in more than 10 points for each sample; signals intensities and minimum acquisition time were used as comparative parameters to determine each platform´s sensitivity.[18] In all cases, the stability of the composites was checked after their use along with their long term stability, with excellent results, as previously demonstrated.[18] For clarity, the two tested families will be described separately in the following sections.

AuZRS@TX systems

View Article Online
DOI: 10.1039/C9CP01896D

Figure 6A shows the minimum acquisition time obtained for *AuZRS@TX* samples when 10 and 20 RS were performed. Systems with 20 RS present lower minimum acquisition times than those with 10 RS, thus a greater sensitivity. This behavior can be related to an increase in the available Au surface when the number of RS is incremented, as it was already reported for *AuZRS@TF* sample.[18] Moreover, a trend in this parameter with respect to film´s mesostructure can be seen: Au loaded TP and TF films present the lower minimum acquisition times while TB films display the highest ones. Also, SERS spectra intensities for *Au20RS@TX* samples (Figure 6B) show that, for the same acquisition time, Au20RS@TP presents higher signal intensities than Au20RS@TF. This is related to the NPs size distribution and amount of Au incorporated in each sample. NPs synthesized in TP and TF films are larger than those synthesized in TB systems, and thus enhance more the Raman signal. In addition, TP films display a greater amount of Au and thus, a larger available surface is expected, giving rise to a higher possibility of signal enhancement. Therefore, these results demonstrate that *AuZRS@TP* samples present the higher sensitivity of all tested platforms, even more than already reported *AuZRS@TF* systems.

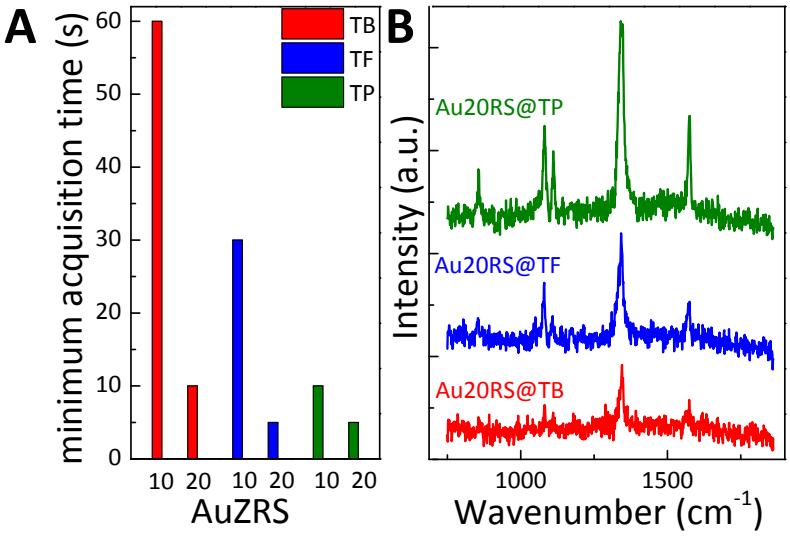

Figure 6. (A) Minimum acquisition time required for S > 3N for *AuZRS@TX* samples. **(B)** SERS spectra of pNTP 10 s acquisition time for *Au20RS@TX* samples. Each spectrum is the average of 4 spectra taken at 4 different points.

Moreover, as can be seen in Figure S8, all *AuZRS@TX* systems presented a highly uniform SERS signal spatial distribution, ideal for routine sensing applications. This spot-to-spot reproducibility can be

View Article Online
DOI: 10.1039/C9CP01896D

attributed to the fact that NPs are evenly synthesized and distributed in the ordered mesoporous matrix. Hence, this SERS signal spatial homogeneity previously reported for *AuZRS@TF* system,[17, 18] is also achieved when P123 and Brij 58 are used as pore templates.

Au66NS/TX systems

In the case of Au NPs covered with TX films, the first observation is that samples prepared with spherical NPs covered with TB and TF films (*Au66/TB* and *Au66/TF*) present very low sensitivity with respect to Au66/TP samples (see Figure S9). This behavior can be explained taking into account the already discussed higher accessibility of TP films to analyte diffusion through necks and pores, allowing a better communication with NPs' surface.

When tips are grown, the obtained *Au66NS/TX* samples present lower minimum acquisition times than the corresponding *Au66/TX* platforms, therefore, a higher sensitivity (Figures 7 and S9). It has been previously shown that growing tips to the NPs generates hot-spots and increases significantly the SERS sensitivity.[15, 18] It is interesting to note, however, that this general behavior is not affected by the pore size and pore structure of the hosting TiO_2 matrix. This means that all the grown tips, independently on their actual sizes, enhance adequately the Raman signal.

Figure 7 shows the minimum acquisition time obtained for *Au66NS/TX* samples alongside the corresponding spectra. In this case, spatial homogeneity is lost, due to the uneven distribution of the Au NPs and each spectra corresponds to the average of 4 different points in a spatial map. There is a clear difference between smaller pores (TB films) and larger pores systems (TF and TP films): the latter present lower minimum acquisition times. Anisotropic NPs in *Au66NS/TF* and *Au66NS/TP* display a more branched structure with longer tips, hence, there is a larger number of hot-spots than NPs in *Au66NS/TB* sample. As a result, the overgrowth of NPs through larger pores produces more sensitive platforms. Nonetheless, the selection of one sensor over another will depend on the desired application. In this way, if high sensitivity is needed, *Au66NS/TP* and *Au66NS/TF* samples will be most accurately chosen. However, if a filtering process is required before sensing, the three platforms will be appropriate depending on the contaminant's size. TP and TF films will be able to filter contaminants with a size larger than 8 nm (*i.e*. proteins)[15] while *Au66NS/TB* samples will be able to filter smaller ones.

View Article Online
DOI: 10.1039/C9CP01896D

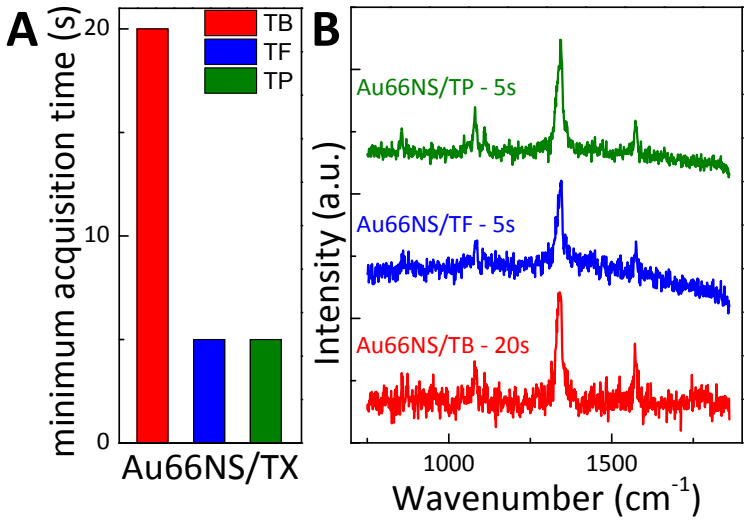

Figure 7. (A) Minimum acquisition time required for S >3N for *Au66NS/TX* samples. **(B)** SERS spectra of pNTP: 20 s acquisition time for Au66NS/TB, and 5 s acquisition time for Au66NS/TF and Au66NS/TP. Each spectrum is the average of 4 spectra taken at 4 different points.

Regarding the comparison with *AuZRS@TX* samples, the *Au66NS/TX* ones present higher signal's intensity but lower signal homogeneity. In this point, it is important to have in mind that the selection of one architecture over another for sensing applications should be done taking into account the desired use.[18] In that sense, it can be envisioned the use of the *AuZRS@TX* platforms for routine SERS determination and the use of the *Au66NS/TX* platforms for traces determination, with different filtering capabilities according to the MTTF pore size.

CONCLUSIONS

In this work, a systematic study about the effect of mesoporous structure over Au NPs growth inside and through the pores of TiO_2 MTFs was presented, and the effect of such characteristics over the composites' sensing capabilities was evaluated.

For that purpose, three different TiO_2 MTFs were prepared, two with the same body-centered cubic pore arrangement (TF and TB) and one with a face-centered cubic one (TP). Additionally, the pore sizes were similar for TF and TP systems and about half in diameter for the TB case.

In a first step, Au NPs were grown inside the pores using an adsorption-reduction approach and it was demonstrated that the amount of incorporated Au and the NPs size is controlled by the pore

View Article Online
DOI: 10.1039/C9CP01896D

array, being higher for the system with face centered cubic array of mesopores (TP). The same structure allowed the growth of more and longer tips over Au NPs deposited in the film/substrate interface. In all cases, TB systems were the less accessible for Au synthesis and overgrowth, due to the smaller pore size. Meanwhile, the body-centered cubic with the bigger pore sizes (TF systems) presented an intermediate behavior.

To test the effect of the structural characteristics over the final composites properties and possible applications, their use as SERS spectroscopy substrates was selected. In such studies, the TP based composites, which include a higher amount of Au or more ramified NPs, were the ones that presented the better sensitivity measured in terms of a probe molecule signal intensity and minimum acquisition time required to detect it. This represents a performance improvement in comparison with the TF based composite substrates previously reported by our group.[18]

Overall, this work demonstrates that the pore size and ordering in MTTFs determine the materials' accessibility for particles' growth and thus has a clear effect over the potential applications of the obtained composites.

ACKNOWLEDGEMENTS

This work has been funded by CONICET (PIP 2012-00044CO), ANPCyT (PICT 2015-0351). The authors acknowledge the CERIC-ERIC consortium for the access to experimental facilities at the Elettra-Sincrotrone Trieste and the financial support. We thank Gonzalo Zbihlei for TEM measurements, Mariana Rosenbusch for EDS measurements and Emilia B. Halac for access to Raman equipment. P. Y. S. and M. M. Z. acknowledge CONICET for their doctoral scholarship.

REFERENCES

1. P. C. Angelomé and M. C. Fuertes, in *Handbook of Sol-Gel Science and Technology*, eds. L. Klein, M. Aparicio and A. Jitianu, Springer International Publishing, Cham, 2018, DOI: 10.1007/978-3-319-19454-7_146-1, ch. 86, pp. 2507-2533
2. P. C. Angelomé and L. M. Liz-Marzán, *J. Sol-Gel Sci. Technol.*, 2014, **70**, 180-190.
3. P. Innocenzi and L. Malfatti, *Chem. Soc. Rev.*, 2013, **42**, 4198-4216.
4. P. Innocenzi and L. Malfatti, *J. Nanopart. Res.*, 2018, **20**, 167.
5. L. Nicole, C. Boissiere, D. Grosso, A. Quach and C. Sanchez, *J. Mater. Chem.*, 2005, **15**, 3598-3627.
6. G. J. A. A. Soler-Illia, P. C. Angelomé, M. C. Fuertes, D. Grosso and C. Boissiere, *Nanoscale*, 2012, **4**, 2549-2566.
7. A. Bonanni, M. Pumera and Y. Miyahara, *Phys. Chem. Chem. Phys.*, 2011, **13**, 4980-4986.
8. X. Jiao, C. Batchelor-McAuley, C. Lin, E. Kätelhön, E. E. L. Tanner, N. P. Young and R. G. Compton, *ACS Catalysis*, 2018, **8**, 6192-6202.

View Article Online
DOI: 10.1039/C9CP01896D

9. R. Álvarez-Puebla, L. M. Liz-Marzán and F. J. García de Abajo, *J. Phys. Chem. Lett.*, 2010, **1**, 2428-2434.
10. Y. Dai, Y. Wang, B. Liu and Y. Yang, *Small*, 2015, **11**, 268-289.
11. Y. Xia, K. D. Gilroy, H.-C. Peng and X. Xia, *Angew. Chem. Int. Ed.*, 2017, **56**, 60-95.
12. Y. Xia, Y. Xiong, B. Lim and S. E. Skrabalak, *Angew. Chem. Int. Ed.*, 2009, **48**, 60-103.
13. R. Gusmão, V. López-Puente, L. Yate, I. Pastoriza-Santos, J. Pérez-Juste and E. González-Romero, *Materials Today Communications*, 2017, **11**, 11-17.
14. S. Schlücker, *Angew. Chem. Int. Ed.*, 2014, **53**, 4756-4795.
15. V. López-Puente, S. Abalde-Cela, P. C. Angelomé, R. A. Alvarez-Puebla and L. M. Liz-Marzán, *J. Phys. Chem. Lett.*, 2013, **4**, 2715-2720.
16. V. López-Puente, P. C. Angelomé, G. J. A. A. Soler-Illia and L. M. Liz-Marzán, *ACS Appl. Mater. Interfaces*, 2015, **7**, 25633-25640.
17. A. Wolosiuk, N. G. Tognalli, E. D. Martínez, M. Granada, M. C. Fuertes, H. Troiani, S. A. Bilmes, A. Fainstein and G. J. A. A. Soler-Illia, *ACS Appl. Mater. Interfaces*, 2014, **6**, 5263-5272.
18. M. M. Zalduendo, J. Langer, J. J. Giner-Casares, E. B. Halac, G. J. A. A. Soler-Illia, L. M. Liz-Marzán and P. C. Angelomé, *J. Phys. Chem. C*, 2018, **122**, 13095-13105.
19. M. Etienne, A. Quach, D. Grosso, L. Nicole, C. Sanchez and A. Walcarius, *Chem. Mater.*, 2007, **19**, 844-856.
20. T.-C. Wei and H. W. Hillhouse, *Langmuir*, 2007, **23**, 5689-5699.
21. M. Etienne, D. Grosso, C. Boissiere, C. Sanchez and A. Walcarius, *Chem. Commun.*, 2005, 4566-4568.
22. S. Sallard, M. Schröder, C. Boissière, C. Dunkel, M. Etienne, A. Walcarius, T. Oekermann, M. Wark and B. M. Smarsly, *Nanoscale*, 2013, **5**, 12316-12329.
23. M. Mercuri, K. Pierpauli, M. G. Bellino and C. L. A. Berli, *Langmuir*, 2017, **33**, 152-157.
24. J. F. Angiolini, M. Stortz, P. Y. Steinberg, E. Mocskos, L. Bruno, G. Soler-Illia, P. C. Angelomé, A. Wolosiuk and V. Levi, *Phys. Chem. Chem. Phys.*, 2017, **19**, 26540-26544.
25. M. A. Carreon, S. Y. Choi, M. Mamak, N. Chopra and G. A. Ozin, *J. Mater. Chem.*, 2007, **17**, 82-89.
26. H.-Y. Lian, Y.-H. Liang, Y. Yamauchi and K. C. W. Wu, *J. Phys. Chem. C*, 2011, **115**, 6581-6590.
27. P. C. Angelomé, I. Pastoriza-Santos, J. Pérez Juste, B. Rodríguez-González, A. Zelcer, G. J. A. A. Soler-Illia and L. M. Liz Marzán, *Nanoscale*, 2012, **4**, 931-939.
28. M. C. Fuertes, M. Marchena, M. C. Marchi, A. Wolosiuk and G. J. A. A. Soler-Illia, *Small*, 2009, **5**, 272-280.
29. G. Kawamura, I. Hayashi, H. Muto and A. Matsuda, *Scripta Mater.*, 2012, **66**, 479-482.
30. L. Bois, F. Chassagneux, C. Desroches, Y. Battie, N. Destouches, N. Gilon, S. Parola and O. Stéphan, *Langmuir*, 2010, **26**, 8729-8736.
31. R. Coneo Rodríguez, M. M. Bruno and P. C. Angelomé, *Sens. Actuators, B*, 2018, **254**, 603-612.
32. Y.-S. Ko and Y.-U. Kwon, *ACS Appl. Mater. Interfaces*, 2013, **5**, 3599-3606.
33. E. D. Martinez, L. Granja, M. G. Bellino and G. J. A. A. Soler-Illia, *Phys. Chem. Chem. Phys.*, 2010, **12**, 14445-14448.
34. J.-Y. Fang, S.-Q. Qin, X.-A. Zhang, Y.-M. Nie and F. Wang, *RSC Adv.*, 2012, **2**, 11777-11785.
35. N. G. Bastús, J. Comenge and V. Puntes, *Langmuir*, 2011, **27**, 11098-11105.
36. C. J. Brinker, Y. Lu, A. Sellinger and H. Fan, *Adv. Mater.*, 1999, **11**, 579-585.
37. E. L. Crepaldi, G. J. A. A. Soler-Illia, D. Grosso, F. Cagnol, F. Ribot and C. Sanchez, *J. Am. Chem. Soc.*, 2003, **125**, 9770-9786.

View Article Online
DOI: 10.1039/C9CP01896D

38. V. R. Koganti, D. Dunphy, V. Gowrishankar, M. D. McGehee, X. Li, J. Wang and S. E. Rankin, *Nano Lett.*, 2006, **6**, 2567-2570.
39. V. M. Sánchez, E. D. Martínez, M. L. Martínez Ricci, H. Troiani and G. J. A. A. Soler-Illia, *J. Phys. Chem. C*, 2013, **117**, 7246-7259.
40. M. Kosmulski, *J. Colloid Interface Sci.*, 2002, **253**, 77-87.
41. S. Y. Choi, B. Lee, D. B. Carew, M. Mamak, F. C. Peiris, S. Speakman, N. Chopra and G. A. Ozin, *Adv. Funct. Mater.*, 2006, **16**, 1731-1738.
42. D. F. Lionello, P. Y. Steinberg, M. M. Zalduendo, G. J. A. A. Soler-Illia, P. C. Angelomé and M. C. Fuertes, *J. Phys. Chem. C*, 2017, **121**, 22576-22586.
43. M. P. Tate, V. N. Urade, J. D. Kowalski, T.-c. Wei, B. D. Hamilton, B. W. Eggiman and H. W. Hillhouse, *J. Phys. Chem. B*, 2006, **110**, 9882-9892.
44. D. Rodríguez-Fernández, P. C. Angelomé, G. J. A. A. Soler-Illia and L. M. C. Liz-Marzán, *Part. Part. Syst. Char.*, 2017, **34**, 1600428.
45. A. Guerrero-Martínez, S. Barbosa, I. Pastoriza-Santos and L. M. Liz-Marzán, *Curr. Opin. Colloid Interface Sci.*, 2011, **16**, 118-127.
46. J. D. Bass, D. Grosso, C. Boissiere, E. Belamie, T. Coradin and C. Sanchez, *Chem. Mater.*, 2007, **19**, 4349-4356.
47. G. Bodelón, V. Montes-García, V. López-Puente, E. H. Hill, C. Hamon, M. N. Sanz-Ortiz, S. Rodal-Cedeira, C. Costas, S. Celiksoy, I. Perez-Juste, L. Scarabelli, A. La Porta, J. Pérez-Juste, I. Pastoriza-Santos and L. M. Liz-Marzán, *Nat. Mater.*, 2016, **15**, 1203-1211.
48. L. Malfatti, P. Falcaro, B. Marmiroli, H. Amenitsch, M. Piccinini, A. Falqui and P. Innocenzi, *Nanoscale*, 2011, **3**, 3760-3766.

View Article Online
DOI: 10.1039/C9CP01896D

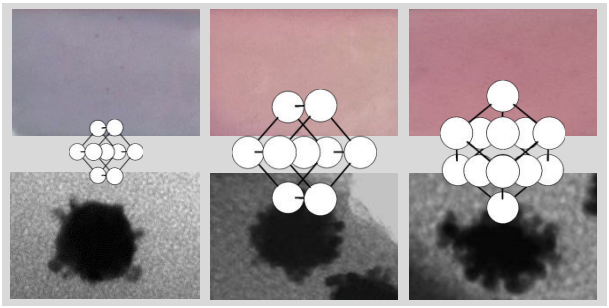

Pore size and ordering in mesoporous TiO_2 thin films defines Au nanoparticles growth through and inside the pores.